

ARTICLE

Open Access

# Ureteral stent sleeve for early detection of hydronephrosis

Nabil Shalabi<sup>1</sup>✉, Kyle Searles<sup>2</sup>, Roman Herout<sup>3,4</sup>, Khaled Almutairi<sup>3,5,6</sup>, Ben H. Chew<sup>3</sup>, Dirk Lange<sup>3</sup> and Kenichi Takahata<sup>1,2</sup>

## Abstract

Hydronephrosis, a serious complication of ureteral stents, can lead to deterioration of renal function due to prolonged increased intrarenal pressure. Currently, the only way to diagnose hydronephrosis is radiographic imaging, and a continuous, non-invasive method is not available. This study introduces the ureteral stent sleeve, UroSleeve, a modular wireless pressure monitoring system that is designed to integrate seamlessly with standard ureteral stents without altering their existing designs or manufacturing processes. The UroSleeve incorporates a flexible printed-circuit-board-based spiral antenna and a surface-micromachined capacitive pressure sensor, forming an inductor-capacitor tank circuit capable of wireless telemetry through near-field inductive coupling. The device was evaluated in an ex vivo porcine kidney model whose internal pressure was externally controlled to mimic a hydronephrosis condition, and kidney pressure changes were successfully monitored by detecting shifts in the resonant frequency of the device. Key results demonstrated a high sensitivity with  $-5.3 \pm 0.74$  kHz/mmHg with a baseline resonant frequency of 15.234 MHz at 8.5 mmHg. The frequency response showed a strong correlation with kidney pressure, and the device maintained consistent performance in a relevant biological environment. The results indicate that UroSleeve offers a practical and versatile solution for wireless intrarenal pressure monitoring, amenable to future clinical translation.

## Introduction

Ureteral stents play a pivotal role in modern urological interventions, serving as indispensable devices in the management of various urinary tract conditions including the treatment of kidney stones, ureteral strictures, and post-surgical interventions<sup>1,2</sup>. These thin, flexible polymeric tubes are routinely deployed by urologists to alleviate obstructions, facilitate urine flow, and promote kidney function<sup>1,2</sup>. Stents typically range from 12 to 30 cm in length and 1.5 to 3 mm in diameter, depending on the specific medical application and patient anatomy<sup>3</sup>. The double-J structure is a common design used in stents, characterized by its curled ends that resemble the letter “J” on both sides<sup>4</sup>. This shape helps anchor the stent in

place, preventing it from migrating while ensuring proper fluid drainage<sup>1,2</sup>.

Despite their numerous benefits, ureteral stents are notorious for post-implantation complications including patient discomfort, urinary symptoms, and, if they stop functioning and the lumen becomes blocked, can cause hydronephrosis (swelling of the kidney) – a late complication due to obstructed urine flow that risks deterioration of renal function due to prolonged elevated intrarenal pressure (average 32.5 mmHg for chronic obstructions, 74.5 mmHg acute, 10.2 mmHg for unobstructed)<sup>5,6</sup>. If the kidney remains obstructed for a prolonged length of time and hydronephrosis persists, this can result in permanent loss of at least some kidney function<sup>7,8</sup>. Earlier identification of hydronephrosis would help clinicians initiate an earlier intervention to perform an operation to change the stent<sup>7,8</sup>. Currently available diagnostic techniques, such as X-rays, computed tomography scans, or ultrasound imaging, lack the ability for continuous, noninvasive, and remote monitoring of patients for early detection of hydronephrosis<sup>7,8</sup>. Recent wearable ultrasound platforms

Correspondence: Nabil Shalabi (nabils@ece.ubc.ca)

<sup>1</sup>Department of Electrical and Computer Engineering, University of British Columbia, Vancouver, BC V6T 1Z4, Canada

<sup>2</sup>School of Biomedical Engineering, University of British Columbia, Vancouver, BC V6T 1Z3, Canada

Full list of author information is available at the end of the article

© The Author(s) 2026



**Open Access** This article is licensed under a Creative Commons Attribution-NonCommercial-NoDerivatives 4.0 International License, which permits any non-commercial use, sharing, distribution and reproduction in any medium or format, as long as you give appropriate credit to the original author(s) and the source, provide a link to the Creative Commons licence, and indicate if you modified the licensed material. You do not have permission under this licence to share adapted material derived from this article or parts of it. The images or other third party material in this article are included in the article's Creative Commons licence, unless indicated otherwise in a credit line to the material. If material is not included in the article's Creative Commons licence and your intended use is not permitted by statutory regulation or exceeds the permitted use, you will need to obtain permission directly from the copyright holder. To view a copy of this licence, visit <http://creativecommons.org/licenses/by-nc-nd/4.0/>.

have also been explored for physiological monitoring, including flexible bladder volume tracking patches<sup>9</sup>, skin-mounted ultrasound arrays that estimate arterial pressure from arterial wall motion<sup>10</sup>, and resonant shell ultrasound devices for pressure inference in compliant vessels<sup>11</sup>. These technologies represent progress in noninvasive monitoring, but they infer pressure or volume indirectly from geometric or resonance-based signatures. In ureteral obstruction, renal pelvis pressure does not exhibit a validated or monotonic ultrasound detectable geometric change, and hydronephrosis-related dilation is nonlinear and varies with renal compliance and obstruction severity<sup>12</sup>. These ultrasound approaches are therefore complementary rather than functionally equivalent to the direct intraluminal pressure quantification targeted by the UroSleeve.

Previous studies attempted to address both direct and remote monitoring by demonstrating an intelligent ureteral stent with a radiofrequency near-field electromagnetic antenna and a micro pressure sensor for resonance-based wireless monitoring of kidney pressure<sup>13–16</sup>. The studies revolved around modifying the structure of existing double-J ureteral stents using laser micromachining to engrave the stents, followed by refilling with copper using electroplating to embed a wireless antenna into the micromachined grooves, and then electrically connecting an off-the-shelf pressure sensor to the antenna<sup>13–16</sup>. While these studies laid the groundwork for advancements in the field, limitations persist due to the invasive manufacturing process, which requires modification of well-established stent manufacturing processes. This design and fabrication approach also limits the size and shape of the antenna and restricts the mechanical flexibility of the modified ureteral stents and custom copper antenna. Flexibility of the stent is necessary for insertion over a guidewire.

This paper aims to fill the critical need for remote monitoring while addressing the limitations in the current research efforts. A proof-of-concept ureteral stent sleeve, named “UroSleeve” in this work, is introduced as a modular solution to wireless pressure sensing that can be adapted to fit snugly over the renal pelvis dwelling region of potentially any type of stent and does not require modifying stent manufacturing technologies. The UroSleeve incorporates an antenna built using flexible printed-circuit-board manufacturing techniques that enable more complex antenna designs at higher resolution, and a Tesla-valve enabled touch mode capacitive pressure sensor inspired by the published switch mode capacitive pressure sensor technology<sup>17</sup>. The modular solution enables cost efficiency, faster adoption, and broader compatibility with different stent types, while reducing risks and regulatory hurdles. This approach simplifies integration into clinical practice, making it a

versatile and practical solution for wireless pressure sensing in ureteral stents.

## Ureteral stent sleeve design

### Working principle

The UroSleeve is placed over a ureteral stent with the pressure sensor located on the renal pelvis dwelling part of the stent such that after implantation, the electrically active device tracks changes in kidney pressure due to hydronephrosis (Fig. 1). The working principle is based on wireless telemetry using the dynamics of an inductor-capacitor circuit (also referred to as an LC tank circuit) embedded into the UroSleeve (transmitter) and excited by an external antenna (reader) using near-field wireless inductive coupling. The spatial proximity between the transmitting entity (the UroSleeve LC tank) and a receiving antenna (a powered external antenna in the form of a reader inductor or a reader LC tank) enables efficient energy transfer and communication by exciting resonance in the UroSleeve LC tank without the need for an onboard power source or battery. The theory of wireless near-field inductive coupling is well described elsewhere<sup>18–20</sup>. Briefly, the resonant frequency of the UroSleeve transmitter,  $f_s$ , is defined as:

$$f_s = \frac{1}{2\pi\sqrt{L_s C_s(p)}}, \quad (1)$$

where  $L_s$  signifies the inductance of the transmitter coil and  $C_s$  signifies the capacitance of the transmitter coil as a function of kidney pressure,  $p$ . The sensitivity of the resultant frequency shift due to the capacitive shift can be related by differentiating the LC tank expression as a function of pressure and is expressed as:

$$\frac{df_s}{dp} = -4\pi\sqrt{L_s} C_s^{\frac{3}{2}} \frac{dC_s}{dp}. \quad (2)$$

Moreover, the quality factor (Q factor),  $Q_s$ , a critical metric characterizing the efficiency of the tank circuit and, consequently, the effectiveness of the wireless telemetry, is expressed as:

$$Q_s = \frac{1}{R_s} \sqrt{\frac{L_s}{C_s(p)}}, \quad (3)$$

where  $R_s$  denotes the parasitic resistance of the tank circuit.

When approached by the external reader antenna, near-field inductive coupling with the UroSleeve LC tank induces a dip in the phase,  $\Delta\varphi_{dip}$ , of the reader antenna at the exact resonant frequency of the UroSleeve LC tank

transmitter. The phase dip can be approximated as:

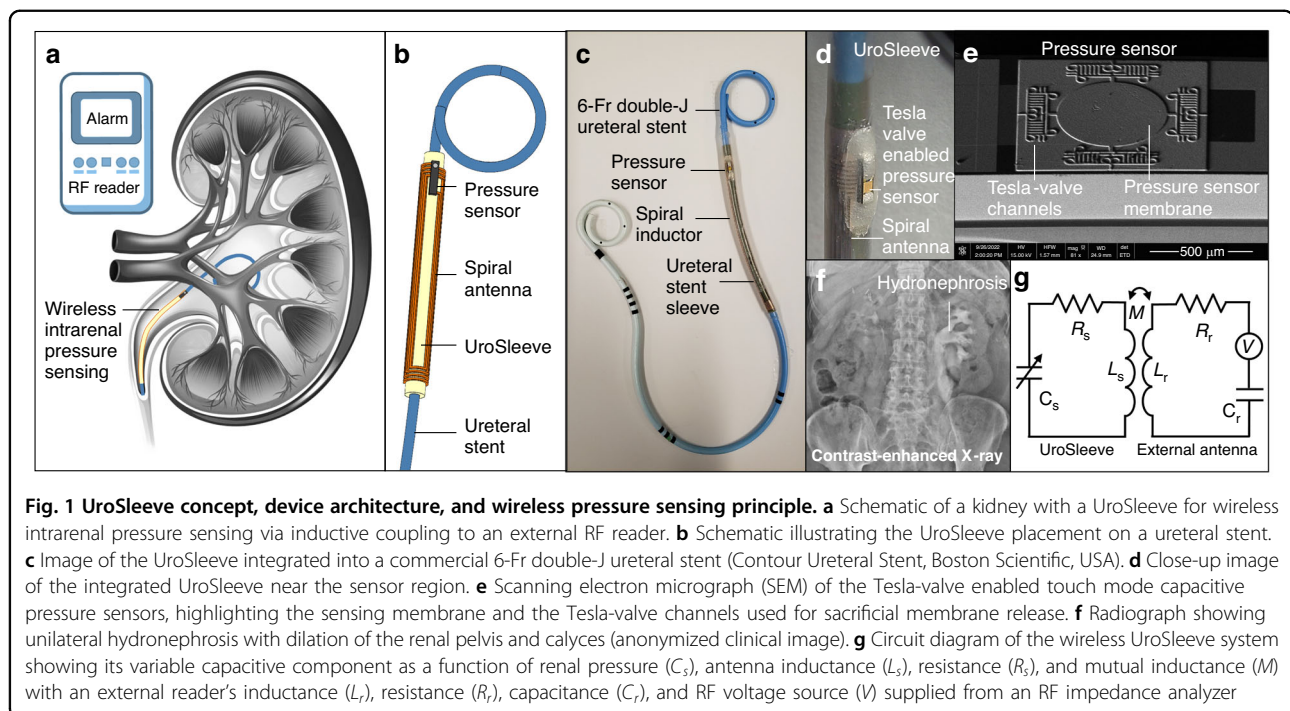
$$\Delta\varphi_{dip} \cong \tan^{-1}\left(\frac{2\pi f_s M^2}{R_s L_r}\right) = \tan^{-1}(Q_s K^2), \quad (4)$$

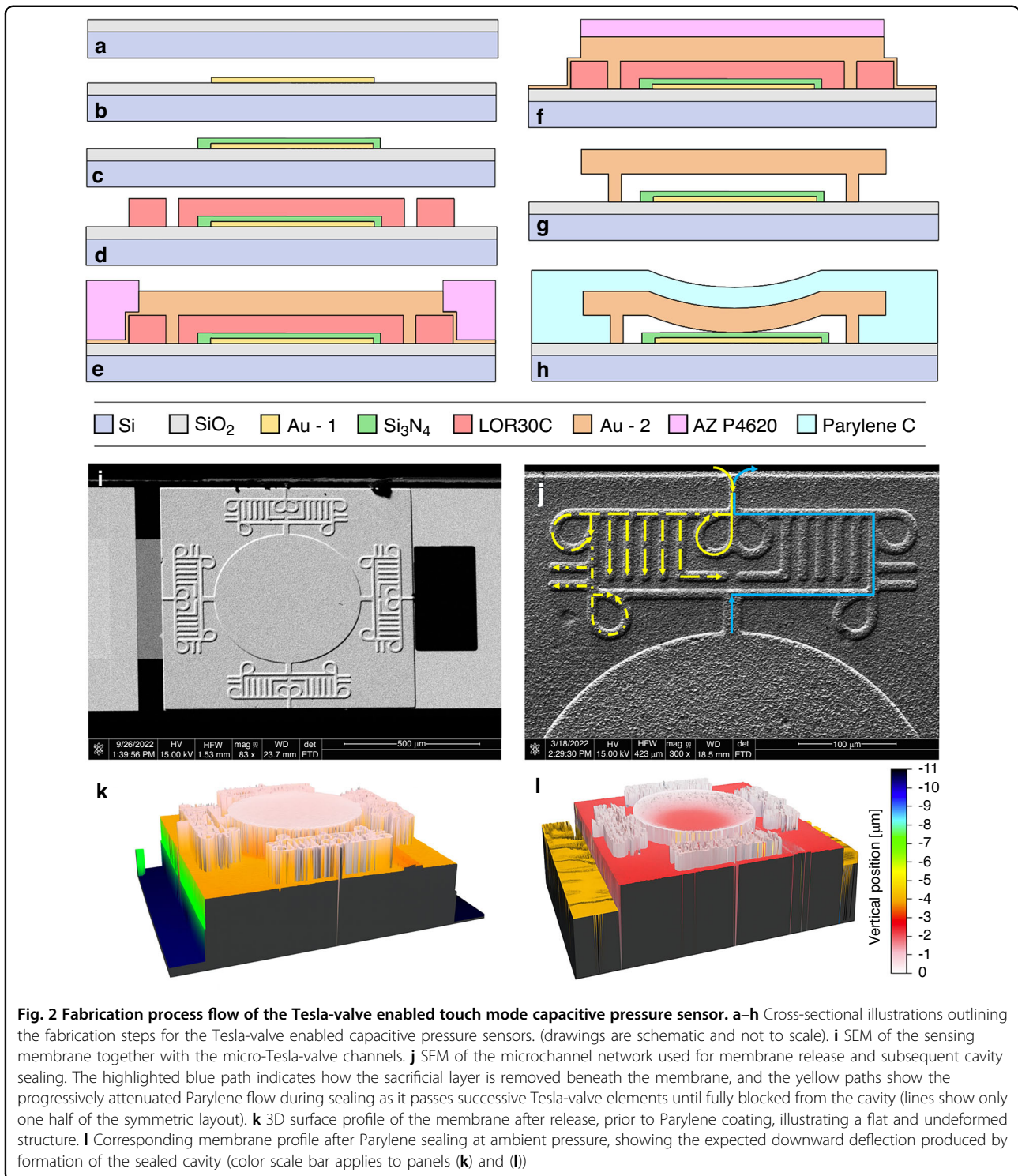
where  $L_r$  represents the inductance of the external reader antenna,  $M$  denotes the mutual inductance between the transmitter's coil and the external reader antenna, and  $K$  is the coupling coefficient.

### Tesla-valve enabled touch mode capacitive pressure sensor

The sensor for renal pelvis monitoring was selected to maximize the capacitive sensing signal relative to changes in renal pelvis pressure. Building on our “switch mode” capacitive pressure sensors reported in<sup>17</sup>, we developed a Tesla-valve enabled “touch mode” capacitive pressure sensor that expanded on the earlier work on this type of sensor pioneered by Ko and Qiang<sup>21,22</sup>, highlighting the versatility of integrating Tesla-valves into pressure sensor technology. This touch mode sensor utilizes a pressure-sensitive membrane as a flexible capacitive electrode where, within the designated pressure range, the membrane comes into contact with a thin dielectric layer covering a stationary counter electrode on the sensor's substrate (see Fig. 2h). As a function of pressure, the contact area of the membrane expands, leading to a corresponding increase in capacitance. Consequently, the touch mode sensor functions

as a pressure-sensitive capacitor that relies on variations in contact area, which results in larger capacitive signals compared to the “normal mode” capacitive pressure sensors that are based on changes in the distance between the capacitive electrodes. The Tesla-valves integrated into the sensor architecture enable the formation of a vacuum-sealed capacitive structure in a more effective and streamlined manner. Briefly, micro-scale Tesla-valves are designed into channels to the capacitive electrode cavity where they enable unidirectional fluidic flow using teardrop-shaped loops, which is pivotal for microfabrication and final packaging. On-chip micro Tesla-valves, with unique channel structures, facilitate cavity sacrificial layer release and sealing through vapor-phase thin-film deposition. The sacrificial layer dissolves in the shortest path opposite to the one-way Tesla-valves during membrane release, preventing residue entrapment. Next, vacuum-sealing the cavity is achieved by biocompatible packaging with Parylene C, where the Tesla-valves block the channels to the membrane before any vaporized Parylene molecules make it to the membrane. While touch mode capacitive pressure sensors commonly rely on a vacuum cavity, the Tesla-valve channels in this design serve two additional purposes beyond standard sealing: (i) They allow the vacuum to be created in situ during the final room-temperature Parylene encapsulation rather than requiring a separate cavity-bonding or wafer-level sealing step<sup>23</sup>, simplifying the overall process, and (ii) they prevent Parylene from depositing





inside the cavity, which would otherwise alter the membrane–electrode gap and reduce the available touch mode capacitance and dynamic range; by preserving a clean, fixed cavity geometry during packaging, the Tesla-valve structure helps maintain the intended sensing characteristics.

The performance of the sensor can be summarized by:

$$C_s(p) = C_{touch}(p) + C_{noncontact}(p) + C_{structural}, \quad (5)$$

where  $C_{touch}(p)$  is the touch mode capacitance from the part of the suspended membrane electrode in contact

with the insulator-coated fixed bottom electrode,  $C_{noncontact}(p)$  is the capacitance from the remaining part of the membrane not in contact with the bottom electrode, and  $C_{structural}$  is the parasitic capacitance from all the structural components of the sensor. The touch mode capacitance is expressed by a circular area integral as:

$$C_{touch}(p) = \int_0^{r_t(p)} \frac{\epsilon_d}{t_d} 2\pi r dr, \quad (6)$$

where  $r$  denotes the polar radial position on the membrane solved within the range from 0 to  $r_t(p)$ ,  $\epsilon_d$  is the dielectric constant of the insulator (silicon nitride) with thickness denoted as  $t_d$ . Upon solving, the touch mode capacitance exhibits a linear increase until membrane deflection begins to saturate, reaching a plateau, as observed in previous studies<sup>21,22</sup>. In contrast, the capacitance  $C_{noncontact}(p)$  is deemed negligible when compared to  $C_{touch}(p)$  because the vacuum cavity thickness significantly exceeds the silicon nitride thickness responsible for the touch mode capacitance (more details on modeling  $C_{noncontact}(p)$  can be found in<sup>24</sup>). Finally, the parasitic capacitance of the sensor is defined as:

$$C_{structural} = \frac{\epsilon_d A_{structural}}{t_d}, \quad (7)$$

where  $A_{structural}$  represents the parasitic capacitance area resulting from the structural components. Table 1 summarizes the chosen sensor design parameters. The sensor chip is configured to have a narrow rectangular shape ( $0.87 \times 3.2 \text{ mm}^2$ ) that is suitable for packaging onto the tubular platform of the UroSleeve with minimal physical projection when aligned in parallel to the axis of the platform.

#### Transmitter spiral antenna and external reader antenna

The inductor of the UroSleeve is based on bending a planar spiral inductor around the cylindrical shape of ureteral stents. Spiral inductors exhibit distinctive electromagnetic fields where the spiral winding gives rise to a concentrated magnetic field influenced by the dimensions and shape of the spiral<sup>19,25</sup>. The theory for spiral inductors is well-established and documented elsewhere<sup>19,25</sup>. Briefly, adjacent coil turns within the spiral electromagnetically couple to generate a more pronounced electromagnetic field and spatial distribution of the magnetic flux. The spiral antenna design considerations include the physical parameters and shape, like the number of turns and dimension, and are selected to maximize the Q factor, via raising its inductance by increasing the spiral length and number of turns while minimizing the resistance by increasing the cross-sectional area of the spiral lines,

**Table 1 Design parameters for the UroSleeve with the integrated antenna and pressure sensor as well as the external reader antenna used –  $\sigma$ : internal residual stress, E: Young’s modulus,  $\nu$ : Poisson’s ratio,  $\epsilon$ : dielectric permittivity R: DC resistance, L: inductance,  $f_r$ : reflectance peak of the external reader antenna**

Parameter	Size [ $\mu\text{m}$ ]	Relevant parameters
Tesla-valve enabled touch mode capacitive pressure sensor		
Sensor chip		
Width	870	
Length	3200	
Substrate thickness	500	
Sensor membrane		
Radius	250	$\sigma$ 26 MPa
Au thickness	2.85 <sup>a</sup>	E 78 GPa, $\nu$ 0.44
Ti adhesion layer thickness	0.02	E 116 GPa, $\nu$ 0.32
Parylene C thickness	4.6	E 2.76 GPa, $\nu$ 0.40
Sensor gap (before deflection)	2.8	
Sensor dielectric		
Sensor dielectric $\text{Si}_3\text{N}_4$ thickness	0.275	$\epsilon$ 9.7 <sup>b</sup>
Tesla-valve channels		
Overall length	178	
Overall width	420	
Channel entrance width	10	
UroSleeve 9 loop spiral antenna		
Length	50,000	R 1.4 ohm, L: 1.97 $\mu\text{H}$ @ 15.1 MHz, $f_r$ 18.1 MHz
Outer spiral width	8270	
Inner spiral width	2110	
Cu Line width	200	
Cu Line thickness	70	
Polyimide substrate thickness	25	
Assembled bend curvature <sup>c</sup>	2790	
External reader 10 loop inductor		
Overall length	50,000	R 0.1 ohm, 4.5 $\mu\text{H}$ @ 16.7 MHz, $f_r$ 28.5 MHz
Overall width	8000	
Wire thickness	510.6	24-gauge magnetic wire

<sup>a</sup>The fabricated sensor had a 2.85- $\mu\text{m}$  thickness based on FEM simulation to place the sensor in touch mode when the sensor cavity is under vacuum

<sup>b</sup>The constant was experimentally measured using the capacitance and the known surface area of characterization structures

<sup>c</sup>The curvature is based on the assembly of a 6-Fr double-J ureteral stent

within the target overall area of  $\sim 8.27 \times 50 \text{ mm}^2$  square. Table 1 summarizes the chosen spiral dimensions based on the dimensional constraints of a 6-Fr (2-mm outside diameter) double-J ureteral stent.

The external reader antenna has a simpler design, as it has no spatial constraints like the UroSleeve, and is based on a looped inductor that is connected to the analyzer for remote tracking of pressure change applied to the sensor. The number of loops on the external reader is chosen to maintain the inductor self-resonance as close as possible above the UroSleeve resonance frequency without hindering the ability to measure variations in the LC tank properties (Table 1).

## UroSleeve fabrication

### Sensor fabrication

The Tesla-valve enabled touch mode sensor was fabricated using a process flow based on the switch mode sensor<sup>17</sup> but with different layer layout designs (Fig. 2). Briefly, a fixed electrode layer is deposited on a silicon wafer (Fig. 2a) through Ti/Au electron-beam evaporation and patterned at 4- $\mu\text{m}$  resolution using a bilayer lift-off process with LOR3A and S1813 photoresists (Fig. 2b). Subsequently, a 275-nm  $\text{Si}_3\text{N}_4$  film is deposited using plasma-enhanced chemical vapor deposition and selectively etched using reactive ion etching with a S1813 patterned photoresist layer (Fig. 2c). A sacrificial layer is then formed by spin coating a bilayer of LOR30C and S1805 photoresists. The bilayer is UV exposed and developed upside down to ensure a positive sidewall profile underneath the S1805, a crucial detail that ensures conformality of a future sputter step. The sacrificial layer is finalized with a 20-second acetone dip that dissolves the S1805 without affecting the LOR30C layer (Fig. 2d). A membrane layer is then created by sputtering Ti/Au (20/300 nm), serving as a seed layer for gold electroplating to complete the membrane. To form an electroplating mold, AZ P4620 photoresist is spin-coated, UV-patterned, and left undeveloped to act as a protective layer during a subsequent wafer dicing step that separates the wafer into  $13 \times 13\text{-mm}^2$  chips. After the dicing, the mold is developed and hard-baked, then individual chips are electroplated in a bath of potassium aurocyanide (Fig. 2e). Post-electroplating, the mold is stripped, and a new pattern of AZ P4620 is applied to etch the Au outside the individual sensors (Fig. 2f) with potassium iodide and a timed Ti etch with 5% hydrofluoric acid. Next, individual sensors are protected with photoresist and diced into microchips. The sacrificial layer is then removed through the micro-Tesla-valve channels with a heated mixture of equal parts acetone and 1165 remover (Fig. 2g). The membrane release process is highly selective, lasting for four days at an elevated temperature without causing structural damage. Chips are then transferred into isopropyl alcohol

to be dried using a critical point dryer. Sensors are electrically connected to the antenna on the polyamide substrate of the UroSleeve. Finally, a 4.6- $\mu\text{m}$  Parylene C coating is conformally applied in vacuum to package the wired sensors and vacuum-seal the cavities by blocking the micro Tesla-valve channels. The sealing process creates a vacuum cavity, which causes the membrane to reflect downwards once the membrane is removed from the parylene coater's vacuum chamber into atmospheric pressure (Fig. 2h). Figure 2i shows an SEM image of the sensor, and Fig. 2j highlights the Tesla-valves and further illustrates the path during membrane release and sealing. Figure 2k, l show white light interferometry images (WLI; Profilm 3D, Filmetrics, CA, USA) of the sensors before and after sealing, showing the membrane entering the touch mode regime once the vacuum is formed and the membrane experiences ambient pressure.

Prior to integration, sensors were conditioned through repeated pressure cycling within the expected operating range to verify basic mechanical robustness and electrical integrity. No visible membrane damage or loss of continuity was observed during assembly or subsequent benchtop testing. The Parylene C coating was selected based on its widespread use in implantable and wearable systems, providing electrical insulation while maintaining biocompatibility<sup>26</sup>.

### Inductor antenna fabrication

The inductor antenna is fabricated using double-sided, adhesiveless copper-clad polyimide (PI) flexible film (Matrix Circuit Board Materials: 70  $\mu\text{m}$  Cu, 25  $\mu\text{m}$  PI, 70  $\mu\text{m}$  Cu). The copper clad of this film is sufficiently thick to effectively reduce the inductor resistance, yet thin enough to remain flexible for wrapping around the stent (the double-sided film was chosen over its single-sided version due to stock availability). One side of the copper is etched away using a copper etchant (CE-100, Transene, USA) after cutting the sheet into a 6.5  $\times$  6.5-inch square and protecting the other side with Kapton tape. Next, the sheet is cut into a 6-inch circle and attached to a 6-inch silicon wafer using a dry film hot roll laminator (XRL-120, Western Magnum, USA) at 110  $^\circ\text{C}$  with a photoresist (AZ P4620, Microchemicals GmbH, Germany) without soft baking. The sheet with the carrier wafer is then spin-coated with the same photoresist (3000 rpm, 500 rpm/sec, 45 sec) followed by baking at 110  $^\circ\text{C}$  for 2 min. Next, the antenna pattern is transferred onto the photoresist using a maskless aligner (MLA 150, Heidelberg, Germany). After taping the sides of the wafer to avoid delamination of the sheet, the photoresist is developed (AZ MIF 300 Developer, Microchemicals GmbH, Germany) for 6 min and then hard baked at 110  $^\circ\text{C}$  for 2 min. Next, the copper is etched upside down with agitation to reach full patterning while monitoring the process in order to prevent over-

etching and achieve the target line width resolution. When finished, the sheet is peeled off the wafer and etch completion is inspected via backside light imaging and electrical resistance measurement. Finally, individual spiral components are cut out to complete the inductor antenna fabrication.

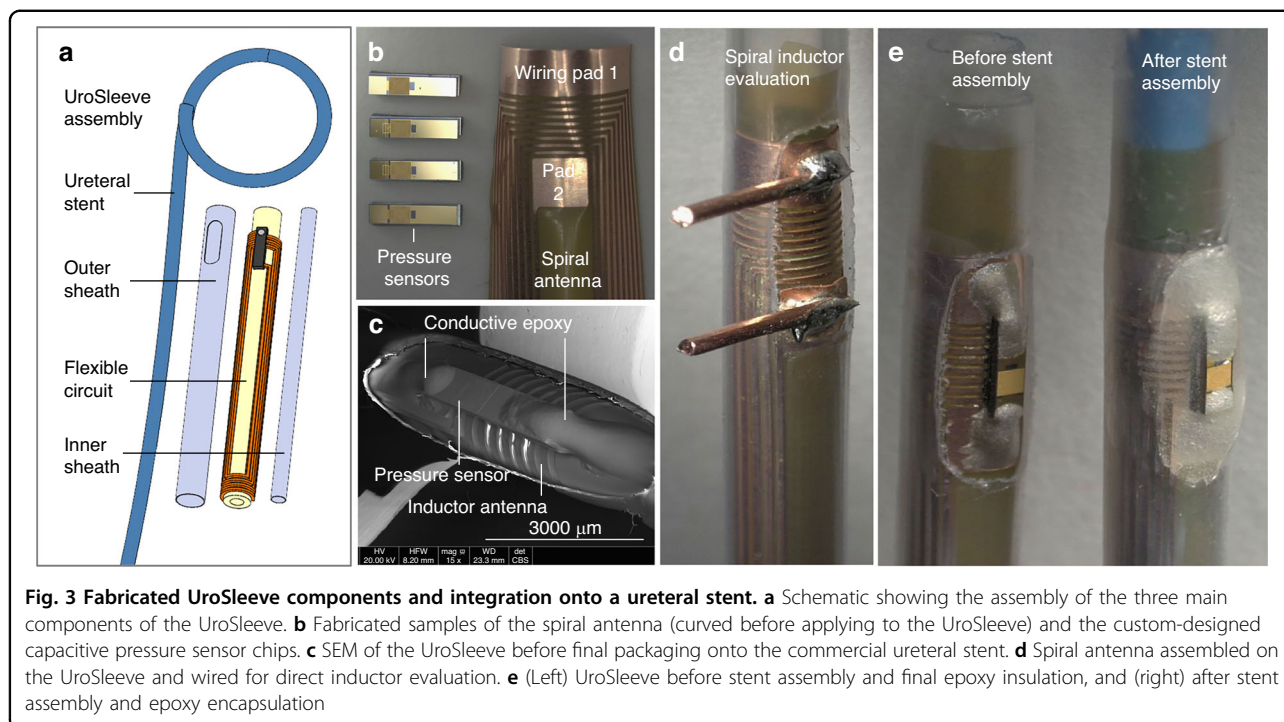
### UroSleeve assembly

The inductor antenna and pressure sensor chip are integrated and packaged into the tubular UroSleeve device. First, the inner surface of the UroSleeve is formed using a fluorinated ethylene propylene (FEP) heat shrink tubing with 2.79-mm to 1.905-mm shrinking diameters (FEP HS. 110 EXP/.075 REC, Zeus, USA) by heating and fitting it onto a metal rod with a diameter of 2.38 mm; the assembly is built onto this temporary rod, instead of directly onto a 6-Fr ureteral stent, to prevent the stent from any thermal damage due to the heating step. Meanwhile, a larger FEP heat shrink tube with 3.581-mm to 2.896-mm shrinking diameters (FEP HS. 140 EXP/.114 REC, Zeus, USA) is prepared by cutting a 2 mm×8 mm oval hole into the tubing using a hole punch to open a space for sensor integration. After wrapping the flexible spiral antenna around the smaller shrink tube assembled onto the metal rod, the larger FEP heat shrink tubing is passed over the spiral antenna and heated to encapsulate it. The outer tubing dictates the final outer diameter of the UroSleeve, which measures at 2.79 mm (8.4 Fr). The pressure sensor chip is then attached to the inductor through the hole in the outer shrink wrap using a

cyanocrylate adhesive (SG3-0.5, ChipQuik, USA) placed under the sensor such that the sensor pads are aligned with the inductor's contact pads. Their electrical connection is secured by tracing lines from the sensor pads to the inductor pads using a low-resistance conductive epoxy (EJ2189-LV, Epoxy technology, MA, USA) with room temperature cure properties (full curing with low contact resistance achieved in 2 days at room temperature). The entire assembly is then coated with Parylene C, after which a high viscosity epoxy is placed inside the outer shrink wrap hole over the sensor connection and sensor itself, and cured while exposing only the sensor membrane (DP110, 3M Scotch-Weld Epoxy Adhesive). The outer heat shrink and the final epoxy step ensure that the UroSleeve is completely insulated from the kidney environment during insertion and operation to prevent any short circuits due to contact with tissue and biological fluids. Finally, the UroSleeve is removed from the temporary metal rod and placed tightly over a 6-Fr double-J ureteral stent (Fig. 1c) with the pressure sensor located on the part of the stent that dwells in the renal pelvis (near the bottom of the stent's renal curl). Figure 3 shows images of the UroSleeve components and fully assembled devices.

### Experimental protocol

The functionality of the UroSleeve was initially evaluated through a wired configuration and then examined wirelessly in air for baseline characterization, followed by testing in an ex vivo model of swine kidney and ureter



immersed in a liquid environment to simulate the pressure buildup through urine obstruction during hydronephrosis (repeated 6 times). Finally, the surface morphologies of the kidney before and after this test were compared to demonstrate the effect of hydronephrosis on the dilation of the ureter.

The ex vivo kidney was surgically extracted from a euthanized pig to excise the kidney and ureter, excluding the bladder, with care taken to maintain the integrity of the renal structures. The renal vein and artery were sutured to seal the kidney, allowing pressure adjustments exclusively through the ureter, which was crucial for monitoring intrarenal pressures during the experiment and for the simulation of hydronephrosis. The extracted kidney was immediately placed in a Krebs solution (containing [mM]: NaCl 130, KCl 4.7, NaHCO<sub>3</sub> 25, MgCl<sub>2</sub> 1.2, dextrose 11, and NaH<sub>2</sub>PO<sub>4</sub> 1.2) chosen for its ability to mimic extracellular fluid and maintain cellular function and viability. The kidney was kept on ice to preserve tissue integrity.

To insert the ureteral stent with the UroSleeve into the ex vivo kidney, a guide wire was inserted into the lumen of the ureter and kidney. The hollow lumen of the stent was then carefully pushed over the guide wire through the ureter into the kidney to ensure proper placement. Afterwards, the guide wire was gently removed and the stent restored the curl for retention inside the renal pelvis with the UroSleeve's sensor situated inside the renal pelvis beyond the ureteropelvic junction. X-ray imaging was performed to confirm the placement of the stent within the kidney and to verify accurate alignment of the UroSleeve with the external antenna (Fig. 4a, b).

To simulate and measure hydronephrosis (Fig. 4c, d, e), a hollow-lumen catheter was passed next to the stent into the renal pelvis and attached to a small chamber connected to an external off-the-shelf pressure sensor and pressure measurement controller (OB1-MK3+ with MPS1, ElveFlow, France). The external sensor was plugged closed from one side and connected directly to the measurement port of the controller. The controller output pressure was also plugged closed as the system was used for its input measurement capabilities (instead of its output pressure control). The small external chamber between the kidney and the external sensor was used to prevent any fluid from getting into the measurement system. After the catheter insertion, the ureter was clamped around the catheter and stent to simulate a ureter obstruction due to a kidney stone. The part of the stent outside the ureter was then fitted with a tight tube connected to a syringe to supply deionized (DI) water into the renal pelvis through the stent and elevate the kidney pressure to simulate the urine buildup in the kidney due to a blocked ureter. Next, the external antenna was covered with a tube to prevent solution and moisture ingress

from shorting the antenna and then connected to an impedance analyzer (4396B, Agilent Technologies, CA, USA). The entire system was submerged in DI water, including the external antenna. The external antenna and the ureter were clamped together to minimize any movement of the ureter so that the measurement results collected were not a result of local movement between the UroSleeve and external antenna, but were a result of elevation in pressure in the renal pelvis. Finally, as the solution was injected into the renal pelvis, while the pressure was recorded through the external reference sensor via the pressure measurement system, the changes in the resonant frequency of UroSleeve were recorded through the phase dip of the reader antenna's impedance (signal monitored every 2.5 seconds at 0 dBm of input power) caused by inductive coupling with the indwelling device.

The recorded data of phase dip frequency as a function of kidney pressure were post-processed using polynomial fitting that captured the profile of the phase dip and accurately extracted the exact dip (minimum) frequency. Furthermore, the Q factor of the inductively coupled LC tanks was measured by analyzing the full width at half maximum (FWHM) of the real part of the impedance (Re(Z)), which is defined as:

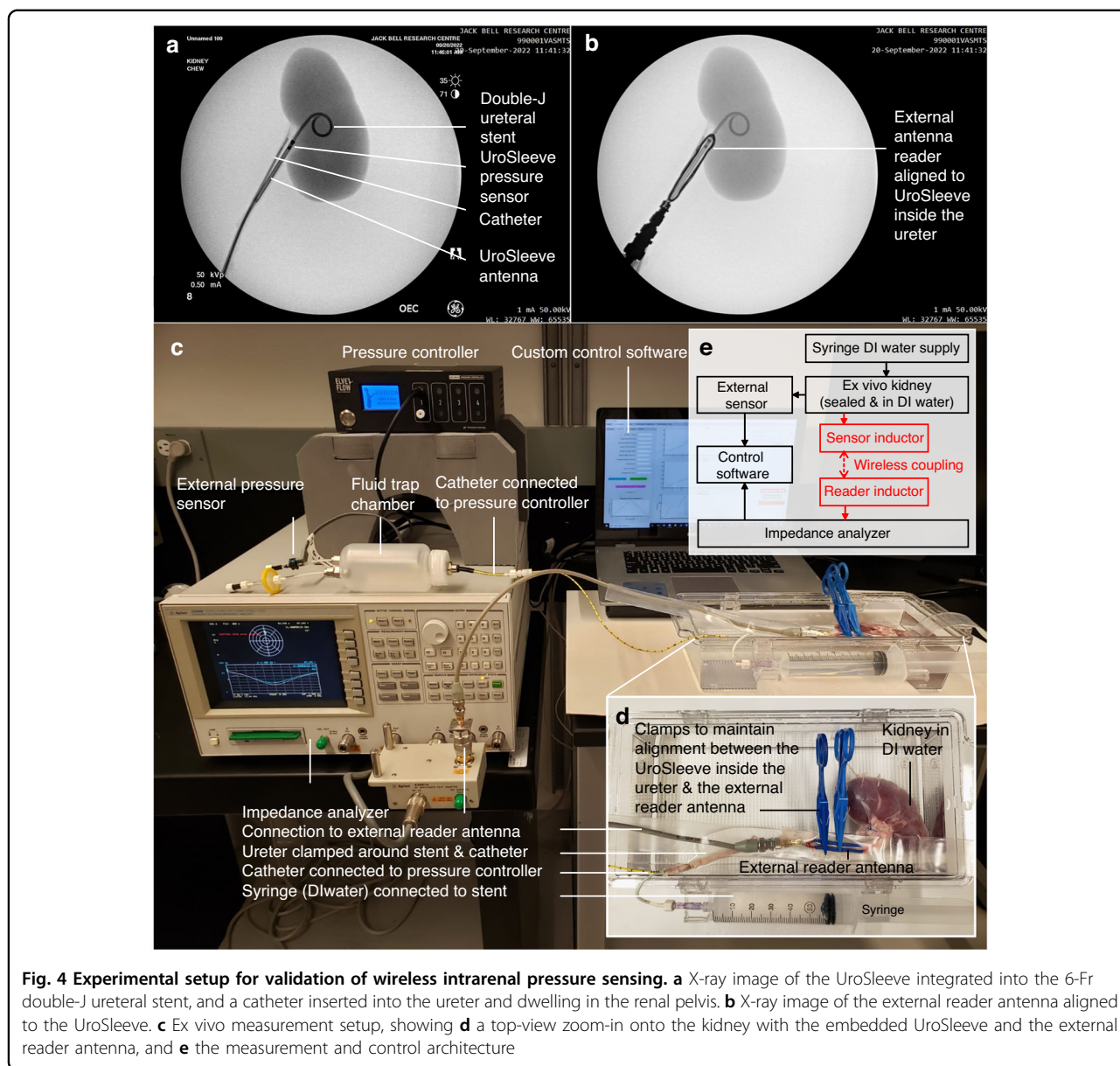
$$Q = \frac{f_s}{\Delta f}, \quad (8)$$

where  $\Delta f$  represents the change in frequency of FWHM of the Re(Z).

## Results

The UroSleeve components were characterized and verified before the final device assembly to get the spiral inductor properties and the custom pressure sensor properties (Fig. 5). The spiral inductors had a 2.003  $\mu$ H inductance at a 15.234 MHz with a self-resonance peak at 185 MHz (Fig. 5a, b). Together with the UroSleeve LC tank had a resonant frequency in air at 18.1 MHz (Fig. 5c). As for the integrated pressure sensors, the baseline capacitance was at  $51.85 \pm 0.00978$  pF at an initial gauge pressure of 0.5 mmHg in air. The capacitive response with a 95% confidence interval is shown in Fig. 5d after pressurizing the sensor to 80 mmHg of gauge pressure. The sensitivity was measured at  $4.4 \pm 0.0451$  fF/mmHg using a linear regression fit with  $r^2$  of 0.996 and standard error of the estimate (SEE) at 0.0063 pF.

A representative result from repeated ex vivo measurements of wireless pressure tracking is illustrated in Fig. 6a. The baseline frequency of the phase dip, caused by the sensor's LC tank resonance, was recorded at  $15.234 \pm 0.07527$  MHz at an initial renal pelvis pressure of 8.5 mmHg (shifted from the LC frequency of 18.1 MHz in



air due to the change in medium). The frequency response with a 95% confidence interval is shown in Fig. 6b after pressurizing the kidney to 56 mmHg. The sensitivity was measured as  $-5.3 \pm 0.74$  kHz/mmHg using a linear regression fit with  $r^2$  of 0.8973 and the SEE at 0.0337 MHz. The Q factor was measured at 4.63 (compared to the Q factor measured in air at 9.8). Finally, after testing, the kidney showed significant signs of hydronephrosis with enlargement of the ureter (hydroureter) and renal capsule distension (Fig. 6c, d).

### Discussion

The ex vivo results demonstrate that UroSleeve can wirelessly track intrarenal pressure, and this work further

shows that Tesla-valve structures can be integrated not only in previously reported switch mode devices<sup>17</sup> but also in the touch mode configuration implemented here, underscoring the versatility of the sensing architecture. The measurements showed a baseline frequency of  $15.234 \pm 0.07527$  MHz at 8.5 mmHg with a corresponding 2.003  $\mu$ H inductance of the spiral antenna, and an observed frequency shift with pressure increase, highlighting the device’s capability to provide accurate readings of pressure change at a sensitivity of  $-5.3 \pm 0.74$  kHz/mmHg. The ex vivo wireless LC results and the UroSleeve antenna inductance allow the calculation of the capacitance of the integrated pressure sensors. At the baseline frequency with a pressure of 8.5 mmHg, the LC tank

calculated capacitance was 54.5 pF (Eq. 1), which is within the range of the measured capacitance in air of the sensor alone (51.9 pF). Based on the frequency sensitivity (Eq. 2), the corresponding ex vivo capacitive sensitivity of the LC tank is calculated to be 35.8 fF/mmHg. This calculated sensitivity to ex vivo kidney pressure is approximately 8 times greater than the sensitivity measured with wired individual sensors in air. Although certain variations in coupling between the UroSleeve and the external reader during pressurization are possible, coupling changes alone would not produce the consistent downward frequency trend observed across all measurements. The strong directionality and monotonicity of the frequency decrease support a pressure-driven mechanism. While enhanced capacitive sensitivity is a favorable characteristic in general, the source of the magnitude difference between wired and ex vivo measurements will need further investigation. We speculate that operating in a high-permittivity aqueous environment differs substantially from air testing and could change the effective electric-field distribution and membrane loading, contributing to the observed outcome. Accordingly, follow-up studies will look into these factors to accurately determine the contribution of environmental effects to the actual sensor response.

In addition, the Q factor measured in ex vivo conditions (4.63) compared to the air (9.8) suggests that the medium substantially influences the resonant properties of the

UroSleeve. This observation aligns with the shift in resonant frequency from 18.1 MHz in air to 15.2 MHz in the ex vivo environment due to a change in the permittivity of the surrounding environment. This Q-factor reduction is expected for passive LC devices operating in conductive, high-permittivity media and, in our measurements, the resonance dip remained readily identifiable across the examined pressure range. The implant Q is fundamentally limited by the biological environment and device scale, and, therefore, future improvements will focus on readout strategies such as phase-sensitive / transient (ring-down) resonance methods<sup>27</sup>, as well as refinement of the external reader-coil geometry and simple alignment aids to improve coupling repeatability, rather than attempting to substantially increase the implant Q.

To compare UroSleeve with previous approaches, earlier smart-stent systems incorporated commercial pressure sensors and LC telemetry directly into the stent wall via laser micromachining and copper refilling<sup>13–16</sup>. These studies demonstrated the feasibility of wireless pressure readout; however, the requirement to remove bulk polymer, pattern metal, and embed rigid sensor components permanently into the stent constrains flexibility, increases the complexity of fabrication, and introduces additional regulatory challenges. By contrast, UroSleeve employs a modular sleeve that preserves the native stent architecture, allowing integration of a custom microfabricated

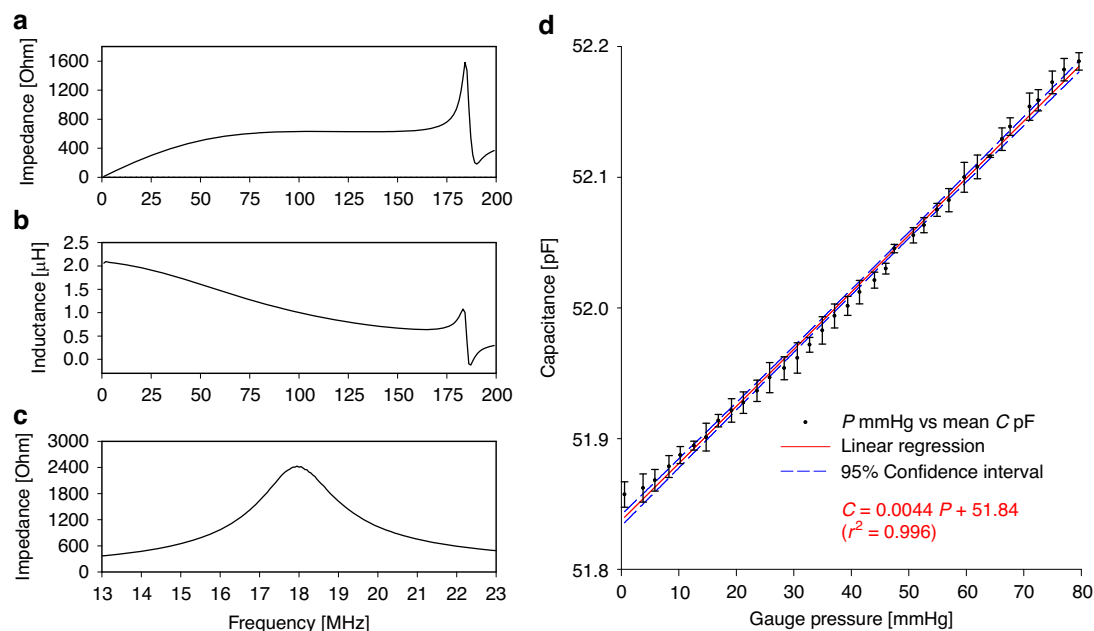
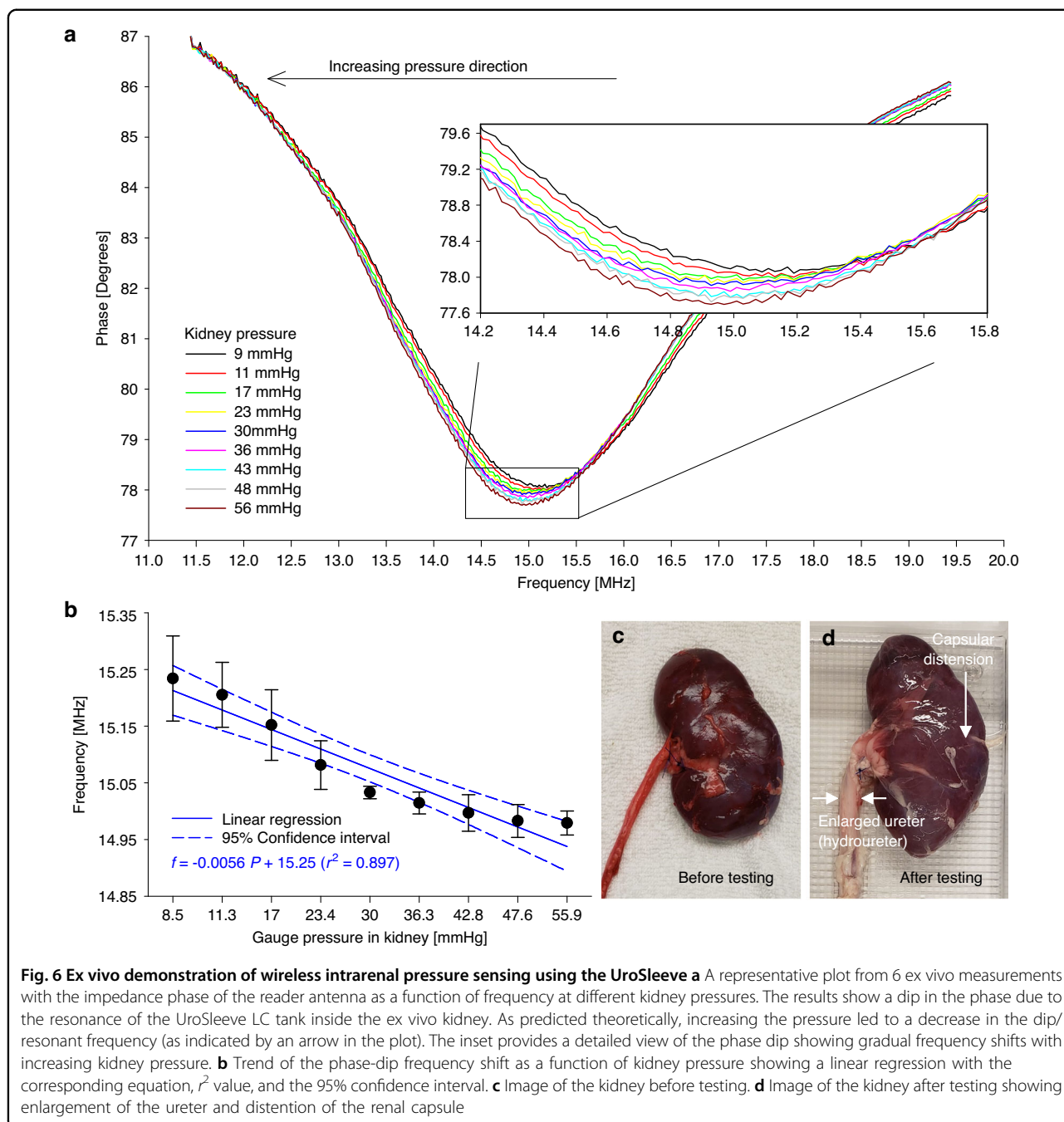


**Fig. 5** Electrical characterization of the spiral inductor, LC tank, and pressure sensor response. **a** Impedance and **b** inductance of the UroSleeve spiral inductor measured as a function of frequency via wired interface in air. **c** Impedance of the UroSleeve LC tank measured as a function of frequency via wired interface in air. **d** Capacitive response of the standalone pressure sensors measured via wired interface as a function of applied pressure in air, showing a linear regression with the corresponding equation,  $r^2$  value, and the 95% confidence interval



sensor without altering stent mechanics or manufacturing pipelines. This separation of sensing element and stent body enables potential adaptation to multiple commercial stent platforms and facilitates future optimization of the sensing chip independent of the stent. We also note that alternative emerging wearable ultrasound systems have been explored for continuous urinary-tract assessment<sup>9–11</sup>; however, these approaches infer functional parameters such as bladder volume or tissue compliance rather than directly measuring renal-pelvis pressure,

making these technologies complementary rather than functionally equivalent modalities.

The current UroSleeve proof-of-concept revealed some limitations and priorities for the next stage of development. First, based on the ex vivo feasibility demonstration, future work will look for long-term evaluation of the UroSleeve system using in vivo models. Planned studies will include repeated longitudinal measurements, including control (no-obstruction) conditions, to map and compensate for possible baseline shift due to

environmental contributions such as tissue loading, medium permittivity, temperature, and aging of the ureteral stent. The effects of urine exposure on the sensed response will also be carefully analyzed and incorporated into future calibration and validation strategies to ensure stable long-term performance. In addition, the influence of the external reader placement will be evaluated under controlled positional offsets to quantify coupling sensitivity and practical alignment tolerances. It is worth noting that although coupling strength may vary with reader position, the resonant frequency, our target signal ( $f_s$  in Eq. 1), is set by the intrinsic LC parameters of UroSleeve, i.e., inherently independent of reader alignment. Accordingly, the reader's positional variation may affect the coupling strength and signal visibility (amplitude and sharpness) but does not shift its frequency, which provides a theoretical basis for robust readout. However, in vivo conditions like those discussed above can shift the true resonant frequency and its baseline signal post-stent placement. In a potential clinical workflow, an initial baseline could be obtained shortly after UroSleeve placement. Follow-up measurements would then be compared to this reference to track the pressure trends. Longitudinal characterization will guide whether simple re-referencing, supplemental reference elements, calibration curves, or alignment aids would further improve robustness in long-term use. Second, full ISO 10993 biocompatibility assessment and long-term encapsulation durability testing will be conducted in vivo. Third, the transition from the current near-field inductive coupling to a far-field telemetry scheme may be necessary to improve longer-distance communication. For example, exploration of alternative resonance measurement techniques could improve the versatility and applicability of the UroSleeve<sup>27</sup>. Fourth, future work could also involve the implementation of the Tesla-valve enabled switch mode pressure sensor<sup>17</sup> as a mitigation strategy to increase the capacitive signal for the same pressure range.

## Conclusion

The UroSleeve offers an advanced and effective approach to addressing the limitations of current ureteral stent monitoring methodologies. Its modular design, along with the demonstrated sensing capability based on a well-established wireless telemetry method, potentially positions it as a valuable tool for improving patient outcomes through timely detection of hydronephrosis through further development and optimization. The ex vivo results provide evidence of the potential of this technology, showcasing its sensitivity and adaptability to biological conditions. Future studies will focus on in vivo testing to validate the UroSleeve's performance by exploring its long-term reliability and biocompatibility for clinical applications. Additionally, integrating this technology with existing healthcare monitoring systems could pave the

way for widespread adoption, ultimately enhancing patient care and reducing healthcare costs associated with ureteral stent complications.

## Acknowledgements

This study was supported by the Canadian Institutes of Health Research (grant no. CPG-158279) as well as the Natural Sciences and Engineering Research Council of Canada (NSERC, grant no. CHRP 523795-18) and partly by CMC Microsystems for our microfabrication work. K.S. was partially supported by an NSERC scholarship. Boston Scientific provided the ureteral stent. The authors wish to thank the following members of the University of British Columbia: Dr. Kostis Michelakis, Dr. Mario Beaudoin, Dr. Andrey Blednov, Khush Dil Hydri, Dr. Matthias Kroug, and Heli Eunike from the Advanced Nanofabrication Facility for their microfabrication support; Dr. Carlos Gerardo for advice and related discussion; Dr. Boris Stoeber for access to his pressure control system; Dr. Mohammad Reza Yousefi Darestani for assistance in lab setup and prior art; Martin Angerer for advice on conductive epoxy.

## Author details

<sup>1</sup>Department of Electrical and Computer Engineering, University of British Columbia, Vancouver, BC V6T 1Z4, Canada. <sup>2</sup>School of Biomedical Engineering, University of British Columbia, Vancouver, BC V6T 1Z3, Canada. <sup>3</sup>The Stone Centre at Vancouver General Hospital, Department of Urologic Sciences, University of British Columbia, Vancouver, BC, Canada. <sup>4</sup>Department of Urology, University Hospital Carl Gustav Carus, Technische Universität Dresden, 01307 Dresden, Germany. <sup>5</sup>King Saud bin Abdulaziz University for Health Sciences, Jeddah, Makkah 22384, Saudi Arabia. <sup>6</sup>King Abdullah International Medical Research Center (KAIMRC), Jeddah, Makkah 22384, Saudi Arabia

## Author contributions

N.S. designed and fabricated the ureteral stent sleeve, planned and conducted experiments, and performed data analysis. K.S. assisted with the design, fabrication, experimental procedures, and software development for testing. R.H. performed the ex vivo organ harvesting. K.A. provided the physiological solution and the recipe used to preserve the ex vivo organs. B.C. and D.L. supervised and advised on all urological aspects of the project. K.T. supervised all aspects of the study. All authors contributed to writing the manuscript, participated in discussions, and finalized the manuscript.

## Conflict of interest

The authors declare no competing interests.

## Ethics declarations

Procedures pertaining to the collection of ex vivo tissue were approved by the Animal Care Committee at the University of British Columbia under Protocol A22-0217.

Received: 5 June 2025 Revised: 4 December 2025 Accepted: 21 January 2026

Published online: 18 March 2026

## References

- Bernasconi, V. et al. Comprehensive overview of ureteral stents based on clinical aspects, material and design. *Cent. Eur. J. Urol.* **76**, 49–56 (2023).
- Sali, G. M. & Joshi, H. B. Ureteric stents: overview of current clinical applications and economic implications. *Int. J. Urol.* **27**, 7–15 (2020).
- Venkatesan, N., Shroff, S., Jayachandran, K. & Doble, M. Polymers as ureteral stents. *J. Endourol.* **24**, 191–198 (2010).
- Finney, R. P. Experience with new double J ureteral catheter stent. *J. Urol.* **120**, 678–681 (1978).
- Geavlete, P. et al. Ureteral stent complications - experience on 50,000 procedures. *J. Med. Life* **14**, 769–775 (2021).
- Cai, Y. et al. A practical pressure measuring method for the upper urinary tract during ureteroscopy. *Clin. Invest Med* **35**, E322 (2012).
- Innes, G. D., Scheuermeyer, F. X., McRae, A. D., Teichman, J. M. H. & Lane, D. J. Hydronephrosis severity clarifies prognosis and guides management for

- emergency department patients with acute ureteral colic, (in eng). *CJEM* **23**, 687–695 (2021).
8. Nestler, S., Grüne, B., Schilchegger, L., Neisius, A. & Jones, J. Evaluation of stone free rates in early versus delayed primary ureteroscopy: time does matter. *World J. Urol.* **39**, 909–914 (2021).
  9. Toymus, A. T. et al. An integrated and flexible ultrasonic device for continuous bladder volume monitoring. *Nat. Commun.* **15**, 7216 (2024).
  10. Zhou, S. et al. Clinical validation of a wearable ultrasound sensor of blood pressure. *Nat. Biomed. Eng.* **9**, 865–881 (2025). (in eng).
  11. Jimenez, R. et al. Resonance sonomanometry for noninvasive, continuous monitoring of blood pressure. *PNAS Nexus* **3**, pgae252 (2024).
  12. Onen, A. Grading of hydronephrosis: an ongoing challenge. *Front. Pediatr.* **8**, 458 (2020).
  13. Yousefi Darestani, M. R., Lange, D., Chew, B. H. & Takahata, K. Electro-mechanically functionalized ureteral stents for wireless obstruction monitoring. *ACS Biomater. Sci. Eng.* **9**, 4392–4403 (2023).
  14. Yousefi Darestani, M. R., Lange, D., Chew, B. H. & Takahata, K. Ex-vivo testing of smart ureteral stent toward hydronephrosis monitoring via standard stenting. in *2024 IEEE Sensors.1–4* (IEEE, 2024).
  15. Yousefi Darestani, M. R., Lange, D., Chew, B. H. & Takahata, K. Intelligent Ureteral Stent Placeable via Standard Procedure for Kidney Pressure Telemetry: An Ex-Vivo Study. *Ann. Biomed. Eng.* **53**, 180–192 (2025).
  16. Yousefi Darestani, M. R., Shalabi, N., Lange, D., Chew, B. H. & Takahata, K. Intelligent ureteral stent for early detection of hydronephrosis. *Adv. Mater. Technol.* **6**, 2100652 (2021).
  17. Shalabi, N., Searles, K. & Takahata, K. Switch mode capacitive pressure sensors. *Microsyst. Nanoeng.* **8**, 132 (2022).
  18. Nopper, R., Niekrawietz, R. & Reindl, L. Wireless readout of passive LC sensors. *IEEE Trans. Instrum. Meas.* **59**, 2450–2457 (2010).
  19. Huang, Q. A., Dong, L. & Wang, L. F. LC Passive Wireless Sensors Toward a Wireless Sensing Platform: Status, Prospects, and Challenges. *J. Microelectromech. Syst.* **25**, 822–841 (2016).
  20. Chen, X., Brox, D., Assadsangabi, B., Hsiang, Y. & Takahata, K. Intelligent telemetric stent for wireless monitoring of intravascular pressure and its in vivo testing. *Biomed. Microdev.* **16**, 745–759 (2014).
  21. Ko, W. H. & Qiang, W. Touch mode capacitive pressure sensors for industrial applications, in *Proceedings IEEE The Tenth Annual International Workshop on Micro Electro Mechanical Systems. An Investigation of Micro Structures, Sensors, Actuators, Machines and Robots*. 284–289 (IEEE, 1997).
  22. Ko, W. H. & Qiang, W. Touch mode capacitive pressure sensors. *Sens. Actuators A Phys.* **75**, 242–251 (1999).
  23. Wan, Y. et al. Wafer-level self-packaging design and fabrication of MEMS capacitive pressure sensors. *Micromachines* **13**, 738 (2022).
  24. Jindal, S. K., Mahajan, A. & Raghuvanshi, S. K. A complete analytical model for clamped edge circular diaphragm non-touch and touch mode capacitive pressure sensor. *Microsyst. Technol.* **22**, 1143–1150 (2016).
  25. Haobijam, G. & Palathinkal, R. P. *Design and Analysis of Spiral Inductors, 2014 edn.* (Springer (India) Private Limited, New Delhi, 2013).
  26. Golda-Cepa, M., Engvall, K., Hakkarainen, M. & Kotarba, A. Recent progress on parylene C polymer for biomedical applications: a review. *Prog. Org. Coat.* **140**, 105493 (2020).
  27. Brox, D. S., Chen, X., Mirabbasi, S. & Takahata, K. Wireless telemetry of stainless-steel-based smart antenna stent using a transient resonance method. *IEEE Antennas Wirel. Propag. Lett.* **15**, 754–757 (2016).